ACS APPLIED MATERIALS & INTERFACES

Research Article

www.acsami.org

Functional Silver Nanoparticle as a Benign Antimicrobial Agent That Eradicates Antibiotic-Resistant Bacteria and Promotes Wound Healing

Xiaomei Dai,[†] Qianqian Guo,[†] Yu Zhao,[†] Peng Zhang,[‡] Tianqi Zhang,[†] Xinge Zhang,*[,†] and Chaoxing Li[†]

[†]Key Laboratory of Functional Polymer Materials of Ministry of Education, Institute of Polymer Chemistry, Nankai University, Tianjin 300071, China

[‡]Department of Chemical Engineering, University of Washington, Seattle, Washington 98195, United States

Supporting Information

ABSTRACT: With the increased prevalence of antibiotic-resistant bacteria infections, there is a pressed need for innovative antimicrobial agent. Here, we report a benign ε-polylysine/silver nanoparticle nanocomposite (EPL-*g*-butyl@AgNPs) with polyvalent and synergistic antibacterial effects. EPL-*g*-butyl@AgNPs exhibited good stability in aqueous solution and effective antibacterial activity against both Gram-negative (*P. aeruginosa*) and Gram-positive (*S. aureus*) bacteria without emergence of bacterial resistance. Importantly, the nanocomposites eradicated the antibiotic-resistant bacteria without toxicity to mammalian cells. Analysis of the antibacterial mechanism confirmed that the nanocomposites adhered to the bacterial surface, irreversibly disrupted the membrane structure of the bacteria, subsequently penetrated cells, and effectively inhibited protein activity, which ultimately led to bacteria apoptosis. Notably, the nanocomposites modulated the relative level of $CD3^+$ T cells and $CD68^+$ macrophages and effectively promoted infected wound healing in diabetic rats. This work improves our understanding of the antibacterial mechanism of AgNPs-based nanocomposites and offers guidance to activity prediction and rational design of effective antimicrobial nanoparticles.

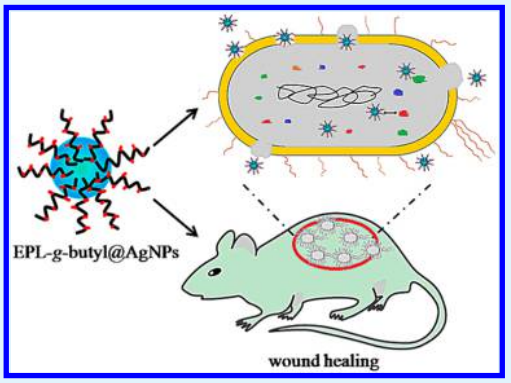

KEYWORDS: *silver nanoparticles, antibiotic-resistant bacteria, wound healing, nanocomposites, antibacterial mechanism*

INTRODUCTION

Throughout the past several decades, the wide and frequent use of antibiotics led to the generation of antibiotic-resistant microorganisms. The resistance to antibiotics in pathogenic bacteria poses a serious threat to global public health if conventional antibiotics are no longer effective.[1] Thus, it is urgent to develop a new antimicrobial agent with safety and strong antimicrobial capability without inducing bacterial resistance. Recently, many antimicrobial agents were reported including polymeric cations,[2,3] quaternary ammonium based compounds,[4] antimicrobial peptides,[5,6] photodynamic/photothermal agents,[7,8] and inorganic nanoparticles.[9−11] Among them, inorganic nanoparticles (NPs) (e.g., silver, copper, and gold NPs) brought new possibilities in the development of effective and safe antimicrobial agents.[12−15] Specifically, silver nanoparticle has been demonstrated to be the most effective antibacterial agent as it has good antibacterial activities against viruses, pathogenic bacteria, and other eukaryotic microorganisms.[16−18] Silver is known to damage the bacterial cell walls and then strongly inhibit enzyme activity by coordinating to electron-donating groups (amides, thiols, hydroxyls, imidazoles, carboxylates, indoles, and so forth), ultimately leading to bacteria apoptosis.[13,19] Moreover, silver displays low cytotoxicity and does not easily trigger the resistance of pathogenic bacteria.[20] Hence, the materials containing silver have been used in catheters, dental materials, implants, wound dressing, and medical devices.[19,20] However, the aggregation of AgNPs to minimize their surface energy will result in a loss of surface area and decrease antimicrobial activity.[20−22] To overcome this limitation, AgNPs can be supported with polymer,[23] such as poly(ethylene glycol)s,[24] poly(vinyl alcohols),[25] poly(vinylpyrrolidones),[26,27] poly(acrylamides),[28,29] polyurethanes,[30] poly(methyl methacrylate),[31] poly(bisphosphonate-*b*-2-vinylpyridine),[32] poly(DL-lactide-*co*-glycolide),[33] poly(styrene−divinylbenzene),[34] polysaccharide,[12] protein,[35] and peptide.[14] However, most of these materials have been restricted by their inherent limitations, such as high cost, poor biocompatibility, complex and tedious preparation procedures, and relatively low targeting efficiency toward bacteria. Hence, a simple method to incorporate silver into biocompatible and biodegradable polymer is desirable.

ε-Polylysine is a naturally occurring polypeptide made of L-lysine, which has been manufactured commercially for its excellent properties such as good water solubility, biocompat-

Received: July 27, 2016
Accepted: September 13, 2016
Published: September 13, 2016

DOI: 10.1021/acsami.6b09267
ACS Appl. Mater. Interfaces 2016, 8, 25798−25807

ibility, and anti-infection activity.[36] In general, the overall hydrophobic/hydrophilic balance of polymer affects antimicrobial activity and selectivity toward bacteria.[37] Our previous study found that ε-polylysine modified with alkyl bromide showed stronger toxicity to bacteria and low cytotoxicity toward NIH3T3 cells.[38] In the present study, we designed a simple and effective peptide−AgNPs binding system, by which an alkylated ε-polylysine was chosen as a bacterial affinity ligand to modify AgNPs. This new antimicrobial peptide−AgNPs composite has a unique advantage to attack bacteria by enhanced multivalent/polyvalent interactions between peptides and lipopolysaccharide moieties on bacteria surface and thus serves as a promising wide-spectrum antibiotic without triggering bacterial resistance. The biodegradable cationic nanocomposites had good cytocompatibility toward NIH3T3 cells and promoted wound healing of the diabetic rats without side effects on dermal tissue.

EXPERIMENTAL SECTION

Materials. ε-Polylysine (EPL, 7000 Da) was purchased from the J&K China Chemical Ltd. (Beijing, China). Butyl bromide and 3-[4,5-dimethylthiazol-2-yl]-2,5-diphenylterazolium bromide (MTT) were purchased from the J&K China Chemical Ltd. (Beijing, China). Anti-CD3 antibody and anti-CD68 antibody were purchased from Abcam (Shanghai, China). Sodium borohydride ($NaBH_4$, 98%), silver nitrate ($AgNO_3$, 99.9%), acridine orange (AO), and ethidium bromide (EB) were gained from Alfa Aesar (Ward Hill, MA). *o*-Nitrophenyl-β-D-galactopyranoside (ONPG) was obtained from Tianjin Heowns Biochem Technologies LLC (Tianjin, China). Streptozocin (STZ) was obtained from Sigma-Aldrich (St. Louis, MO). *Escherichia coli* (*E. coli*) ATCC 8739, *Pseudomonas aeruginosa* (*P. aeruginosa*) ATCC9027, *Staphylococcus aureus* (*S. aureus*) ATCC 6538, and antibiotic-resistant strains were obtained from the Department of Microbiology of Nankai University (Tianjin, China). The other chemicals were analytical reagents and used without purification.

Synthesis and Characterization of Alkylated ε-Polylysine (EPL-*g*-Butyl). Typically, EPL (0.5 g) was dissolved in dimethyl sulfoxide (DMSO) (10 mL), and 4 mL of 1 mol/L sodium hydroxide (NaOH) was added over 2 h at 50 °C. Then butyl bromide (2.0 mmol) was added. After the mixture was stirred for 24 h at 60 °C, the obtained EPL-*g*-butyl was finally purified by dialysis against deionized (DI) water. The structure of EPL-*g*-butyl was assayed by ^{1}H NMR (Bruker AVANCE III 400 MHz NMR) and FT-IR (America, Biorad). After alkylation, the peaks at 0.85, 1.3, and 3.5 ppm in ^{1}H NMR spectrum were characteristic of $-CH_3$, $-NH[CH_2-(C\underline{H}_2)_2-CH_3]$, and $-NH[C\underline{H}_2-(CH_2)_2-CH_3]$ attributed to butyl chains, indicating successful alkylation of EPL (Figure S1). In FT-IR spectra, comparing with EPL, the prominent peaks at 2920 and 2852 cm^{-1} in alkylated EPL were assigned to the C−H stretching vibration, suggesting the presence of *N*-alkyl substitution. Also, the bands at about 1461 cm^{-1} attributed to C−H bending were intensified after alkylation (Figure S2). The degree of substitution was about 23% as estimated by elemental analysis.

Preparation of EPL-*g*-Butyl@AgNPs. EPL-*g*-butyl@AgNPs was prepared according to the previous method with slight modifications.[13] 37.5 μL of 58.8 mmol/L $AgNO_3$ and 0.37 μmol of EPL-*g*-butyl were mixed with 2 mL of DI water under stirring. Then, 55 μL of 312 mmol/L fleshly $NaBH_4$ was quickly added, and the solution was continued to stir for 30 min. The color of the solution was evolving from yellow to brown, suggesting the formation of AgNPs. The concentration of EPL-*g*-butyl@AgNPs was 1.5 mg/mL.

Characterization of AgNPs and EPL-*g*-Butyl@AgNPs. UV−vis spectroscopy was used as an analytical tool to track AgNPs formation. The morphology of the obtained nanocomposites was observed using a transmission electron microscope (TEM). A droplet of EPL-*g*-butyl@AgNPs was placed on an ultrathin carbon film and dried at room temperature before observation. X-ray photoelectron spectroscopy (XPS) was performed to evaluate the weight percentage of NPs in the selected nanocomposites. X-ray diffraction (XRD) was detected on an X-ray diffractometer (Rigaku, D/max-2500 using a Cu tube).

Silver Ion Release. To monitor the silver ion release, EPL-*g*-butyl@AgNPs (4 mL, 6 mg/mL) and AgNPs (4 mL, 5.3 mg/mL) with the same amount of silver were transferred to a dialysis tube (3.5 kDa, cutoff) and dialyzed against 25 mL of DI water at 37 °C. The solution was collected every 2 h for the first 12 h, and the dialysis tube containing the nanocomposites was refilled with an additional 25 mL of DI water each time. The solution was obtained and determined by an inductively coupled plasma mass spectrometer (ICP-MS, Thermo Electron Corporation).

Antibacterial Activity. The minimum inhibitory concentration (MIC) of the antimicrobial agent was determined according to the previous method with minor modification.[14] Bacteria were incubated in Luriae Bertani (LB) broth at 37 °C overnight. The nanocomposite suspension and the bacterial suspension (2×10^7 CFU/mL) were mixed and then cultured for 8 h at 37 °C. The OD_{600} value of the solution was measured using UV−vis absorption to determine the amount of bacteria. Each assay was carried out in triplicates.

The in-vitro synergistic action of the compound A (EPL-*g*-butyl) and compound B (AgNPs) was investigated using a two-dimensional microdilution assay.[39] The fractional inhibitory concentration (FIC) was calculated as follows:

$$\mathrm{FIC} = \frac{\text{MIC of compound A in combination}}{\text{MIC of compound A alone}} + \frac{\text{MIC of compound B in combination}}{\text{MIC of compound B alone}}$$

The interaction of compounds A and B was defined as synergistic action if the FIC index was ≤0.5.[40]

The zone of inhibition was further used to determine the synergistic antibacterial action between AgNPs and EPL-*g*-butyl. The bacterial suspension (5×10^7 CFU/mL) was inoculated evenly on an LB agar plate. The sample disk with a diameter of 8 mm containing the antibacterial materials was placed on the LB agar plate and cultured for 10 h. The antimicrobial activities were assayed by measuring the diameter of the zone of inhibition around the disks in triplicates.

The bacterial death assay was also determined by fluorescent-based cell live/dead method. 1.5 mL of the bacterial cells (5×10^7 CFU/mL) was collected and rinsed with PBS (pH 7.4). The suspension was treated with EPL-*g*-butyl@AgNPs above MIC (25 μg/mL for *S. aureus* and 50 μg/mL for *P. aeruginosa*), and untreated bacteria were taken as control.[41] After the mixture cultured at 25 °C for 1 h, 100 μL of fluorescent dyes was added to the cells and incubated for further 15 min. All samples were observed under an inverted fluorescence microscope (Leica DMI 4000B). The sample without EPL-*g*-butyl@AgNPs was used as a control.

Inhibition Assay of Enzyme β-Galactosidase Activity. 50 mL of *E. coli* suspension (5.0×10^8 CFU/mL) was obtained by centrifuging (5000 rpm) and washed three times. The cytoplasm solution was obtained from the *E. coli* suspension.[13] Then, the solution containing the cytoplasm (1.0 mL) was incubated with different concentrations of EPL-*g*-butyl@AgNPs (0.9, 1.8, and 3.6 μg/mL) and AgNPs (1.8 μg/mL). The same amount of the solution without EPL-*g*-butyl@AgNPs was used as control. Then, *o*-nitrophenyl-β-D-galactopyranoside (ONPG) was added, and the *o*-nitrophenol (ONP) was recorded at 420 nm (OD_{420}) using UV−vis spectroscopy. Each test was carried out three times.[42] The percentage of β-galactosidase inhibition was calculated using the following equation:

$$\text{inhibition } \% = \frac{OD_{420}(\text{control}) - OD_{420}(\text{sample})}{OD_{420}(\text{control})} \times 100\%$$

Morphological Characterization of Bacteria. The bacterial suspension (5.0×10^7 CFU/mL) was collected and washed three times. The suspensions were cultured with EPL-*g*-butyl@AgNPs (75 μg/mL) for 1 h. The treated cells were centrifuged (5000 rpm) at 4 °C for 5 min and washed with PBS. The bacteria without treated was used as control. All bacteria cells were fixed on the glass with 2.5%

DOI: 10.1021/acsami.6b09267
ACS Appl. Mater. Interfaces 2016, 8, 25798−25807

glutaraldehyde solution for 12 h, washed with PBS, dehydrated with sequential treatment of 30%, 50%, 70%, 90%, 95%, and 100% ethanol solution for 10 min, and dried under vacuum.[13] The samples were coated with platinum and then imaged by a scanning electron microscope (SEM; Shimadzu SS-550).

Induction of Bacterial Resistance. The bacterial suspension (1.0×10^7 CFU/mL) was cultured with 1/2 MIC of EPL-*g*-butyl@AgNPs or levofloxacin at 37 °C. After the concentration of bacteria reached 2.0×10^7 CFU/mL, the bacteria was cultured on agar plates with the nanocomposites or levofloxacin; susceptibility to nanocomposites or levofloxacin was evaluated by MIC assay. The cultures were passaged 30 times to obtain resistant variants, and the MIC was determined after each passage.

Cytotoxicity Assay. MTT assay was used to evaluated the cytotoxicity of EPL-*g*-butyl@AgNPs. NIH3T3 cells, as the cell model, were seeded into 96-well plates at about 1.0×10^4 cells per well in 100 μL of Dulbecco's Modified Eagle's Medium (DMEM) supplemented with 10% fetal bovine serum and further incubated at 37 °C for 24 h in 5% CO_2/95% air. EPL-*g*-butyl@AgNPs was diluted using culture medium to gain the required concentrations (1.8, 3.5, 7, 14, and 28 μg/mL). All NIH3T3 cells were treated with various concentrations of EPL-*g*-butyl@AgNPs for another 1 or 2 days, and the cell viability was analyzed using the MTT method as previously described.[43,44] The cells without treatment of EPL-*g*-butyl@AgNPs were used as control, and their cell viability was set at 100%. Each sample was repeated five times.

***In Vivo* Study.** Male Wistar rats (250−300 g body weight) were obtained from Beijing HFK Bioscience Co., Ltd. All rats were individually raised in cages on a 12:12 L/D cycle (lights on at 7 a.m.) under standardized temperature. Diabetic rats were induced by an intravenous injection of streptozotocin (STZ) (45 mg/kg) into the fasting rats. Rats were defined as having insulin-dependent diabetes mellitus (IDDM) when their plasma glucose concentrations was up to 16.7 mmol/L.[45] All experiments were carried out 4 days later of STZ injection. The animals were anesthetized by 10% chloral hydrate (30 mg/kg), and then four wounds were prepared on the right and left sides of the backbone of rat with a surgical scalpel, over a surface of circle (diameter of 1.5 cm).[13] The wounds were divided into four groups: treatment group (Group I), model group (Group II), nanocomposite control group (Group III), and blank control group (Group IV). 150 μL of the bacterial mixture (suspension of equal volume and concentration of Gram-negative (*P. aeruginosa*) and Gram-positive (*S. aureus*) bacteria, 2.0×10^7 CFU/mL) was used to infect the tissue of treatment group and model group. After 3 days, the pus was observed on the infected wound of treatment group and model group. 150 μL of 28 μg/mL EPL-*g*-butyl@AgNPs or AgNPs was smeared on the wounds of treatment group and nanocomposite control group once a day and continued for 18 days. The wounds of blank control group were treated with 150 μL of 0.9% NaCl solution every day, while the wounds of model group were subjected to no disposal. After 18 days of administration, wound recovery was observed and the tissue samples were obtained to prepare pathological slides. Hematoxylin and eosin (H&E)-stained histological images were obtained by a Nikon Eclipse TE2000-U microscope.

Immunohistochemical Analysis. Immunohistochemistry analysis exploited the principle of antibodies binding specifically to antigens. The visualized color changing reaction of the antibody is commonly accomplished by conjugating an enzyme to the antibody. This method can exactly show where a given protein is located. The expression of $CD3^+$ and $CD68^+$ was used for analysis of T cells and macrophage, respectively. Antigen retrieval was carried out on paraffin embedded sections before dual staining for these cells.[46]

Statistical Analysis. All data are evaluated as means ± standard deviation of three or five tests and contrasted via Kruskal−Wallis one-way analysis of variance (ANOVA); $*p < 0.05$ (extremely significant).

RESULTS AND DISCUSSION

Preparation and Characterization of EPL-*g*-Butyl@AgNPs. Since the antimicrobial activity and cytotoxicity of cationic polymers are related to the length of the alkyl tail,[13,38] EPL was modified with different alkyl bromides. We systematically investigated the impact of the length of alkyl chain on antibacterial activities and cytotoxicity of the polymers and found that EPL-*g*-butyl with a substitution degree of 23% showed stronger toxicity to bacteria and lower cytotoxicity toward NIH3T3 cells.[38] Thereby, in the present work, this alkylated EPL was chosen as the polymer support to achieve a stable suspension of AgNPs in the aqueous solution. EPL-*g*-butyl@AgNPs were prepared by reduction of $AgNO_3$ with $NaBH_4$ in EPL-*g*-butyl solution (Scheme 1). To systematically

Scheme 1. Synthetic Scheme of EPL-*g*-Butyl@AgNPs

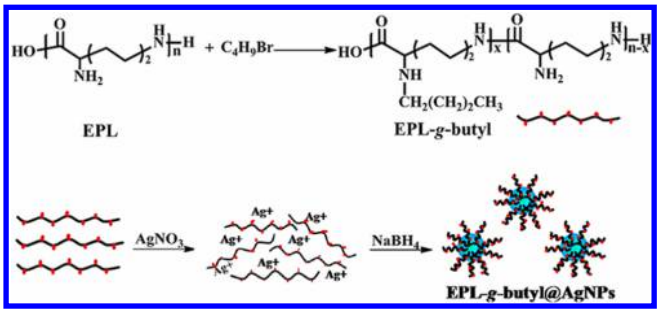

investigate the effect of surface chemistry of nanocomposites on antimicrobial efficacy, EPL-*g*-butyl@AgNPs with different molar ratios of EPL-*g*-butyl to silver ion (1:4, 1:8, 1:16, 1:32, and 1:64) were prepared. The color of nanocomposites turned from yellow to brown as the molar ratios increased (Figure 1A). Unlike AgNPs suspension which aggregated easily, EPL-*g*-butyl@AgNPs solutions were stable at 25 °C for up to six months, indicating that EPL-*g*-butyl can effectively stabilize AgNPs. The size of the nanocomposites with different molar ratios of EPL-*g*-butyl to silver ion (1:4, 1:8, 1:16, 1:32, and 1:64) is shown in Figure S3. There was no significant difference between them. To further confirm the synthesis of nanocomposites, we determined their absorption using UV−vis spectroscopy. The absorption peak of nanocomposites displayed red-shifted compared with AgNPs (396 nm), indicating the formation of EPL-*g*-butyl@AgNPs (Figure 1B). The morphology of EPL-*g*-butyl@AgNPs observed under TEM showed that the inner AgNPs were spherical with a diameter of about 7 nm (Figure 1C), and the hydrodynamic diameter determined by DLS displayed that the nanocomposites were well dispersed in aqueous solution with a diameter of 17.8 nm (Figure 1D). The chemical compositions and electronic structures of EPL-*g*-butyl@AgNPs were further analyzed by XPS. The peaks of C, N, O, and Ag in the sample were clearly observed (Figure 1E). The XPS spectrum of Ag 3d showed that the binding energies of Ag $3d_{3/2}$ and Ag $3d_{5/2}$ peaks at 373.5 and 367.4 eV, respectively (inside). The dehiscence of the 3d doublet was 6.1 eV, suggesting the metallic nature of Ag. The Ag 3d peak shifted to lower binding energy, suggesting that AgO existed in the nanocomposites.[47] XRD analysis was used to investigate the crystalline structure of EPL-*g*-butyl@AgNPs (Figure 1F). The peaks obtained at 37.96°, 44.16°, 64.32°, and 77.42° were assigned to (111), (200), (220), and (311) reflections, respectively. The result confirmed that AgNP crystals presented cubic structure. We further evaluated the antimicrobial activities of EPL-*g*-butyl@AgNPs against Gram-positive and Gram-negative bacteria. As shown in Figures 1G and 1H, the bacterial viability decreased with increasing the

DOI: 10.1021/acsami.6b09267
ACS Appl. Mater. Interfaces 2016, 8, 25798−25807

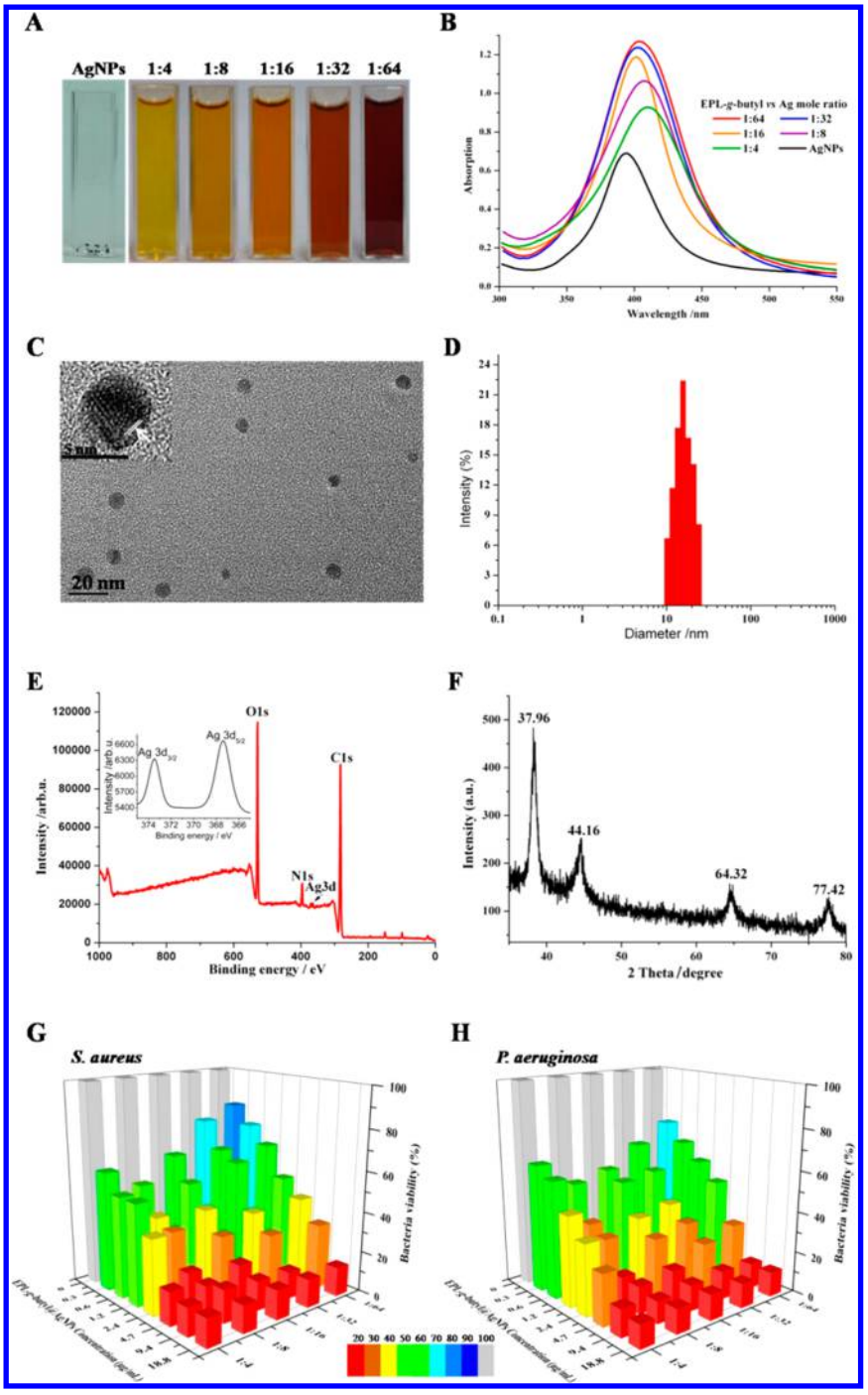

Figure 1. Characterization of the EPL-*g*-butyl@AgNPs with different EPL-*g*-butyl to AgNPs ratios: (A) Photographs of EPL-*g*-butyl@AgNPs and AgNPs in aqueous solution; (B) UV−vis absorption spectra of AgNPs and EPL-*g*-butyl@AgNPs; (C) TEM image of EPL-*g*-butyl@AgNPs (1:8); (D) diameter distribution of EPL-*g*-butyl@AgNPs (1:8) in aqueous solution; (E) XPS photographs of EPL-*g*-butyl@AgNPs (1:8). Ag 3d core level spectrum of EPL-*g*-butyl@AgNPs (inset); (F) XRD pattern of EPL-*g*-butyl@AgNPs (1:8); (G) antibacterial effect of different ratios of EPL-*g*-butyl to AgNPs for *S. aureus*; (H) antibacterial effect of different ratios of EPL-*g*-butyl to AgNPs for *P. aeruginosa*.

nanocomposite dosages. The nanocomposites with 1:8 molar ratio of EPL-*g*-butyl to silver ion showed the best performance with MIC value of 2.4 μg/mL to both *S. aureus* and *P. aeruginosa*. Hence, this nanocomposition was chosen as the representative in the following tests.

Silver Ion Release. ICP-MS analysis was used to assess the potential release of silver ions. As shown in Figure 2, both EPL-*g*-butyl@AgNPs and AgNPs showed a maximum Ag^+ release within first 2 h (8.5 and 10.5 μg/L, respectively) and then decreased in the following time. At 6 h, AgNPs released less (2.4 μg/L) Ag^+ than EPL-*g*-butyl@AgNPs (4.9 μg/L) due to the occurrence of AgNPs precipitation. After 12 h, the release of Ag^+ from EPL-*g*-butyl@AgNPs reached a constant level (about 2.5 μg/L), indicating that EPL-*g*-butyl@AgNPs provided a slow and sustained Ag^+ release.

Antibacterial Activity of EPL-*g*-Butyl@AgNPs. The functional ligands on nanoparticle surface can provide direct multivalent interaction to biological molecules, allowing the

DOI: 10.1021/acsami.6b09267
ACS Appl. Mater. Interfaces 2016, 8, 25798−25807

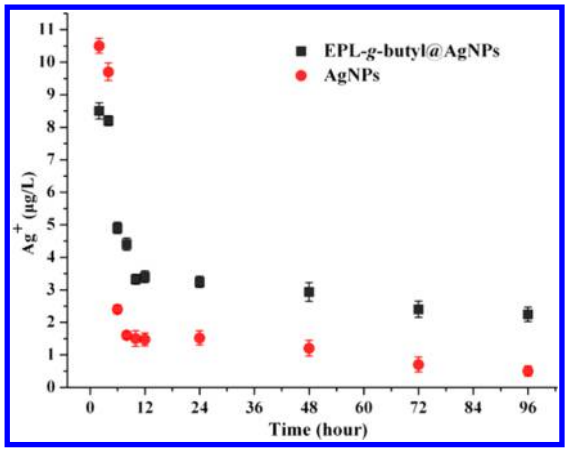

Figure 2. Release of silver from EPL-*g*-butyl@AgNPs and AgNPs after sequential washing steps with 25 mL of DI water. For the first 12 h, EPL-*g*-butyl@AgNPs and AgNPs were washed every 2 h. After 24 h, the washing process was performed with a 24 h time interval.

nanocomposites to be exploited as self-therapeutic agents.[48,49] Multivalent interactions describe the interaction between multivalent receptors and ligands,[50] including protein−carbohydrate interactions,[51] electrostatic interactions, and hydrophobic and hydrophilic interactions.[52]

As shown in Figure 3, when the concentration of EPL-*g*-butyl@AgNPs reached 4.7 μg/mL, the growth of antibiotic-

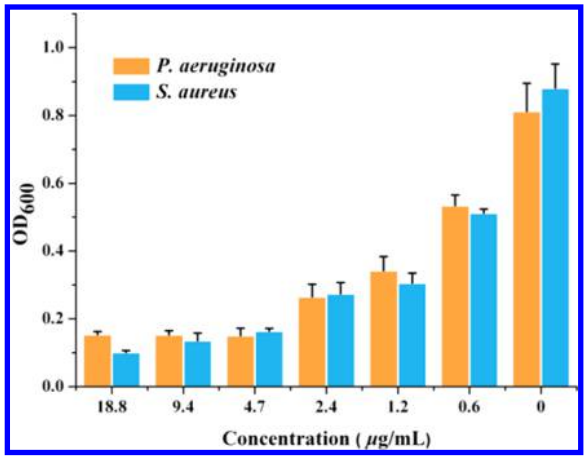

Figure 3. Antibacterial activity of EPL-*g*-butyl@AgNPs against antibiotic-resistant *P. aeruginosa* and *S. aureus*.

resistant Gram-negative (*P. aeruginosa*) and Gram-positive (*S. aureus*) bacteria was significantly inhibited. Additionally, the zone of inhibition test was also carried out to investigate the antimicrobial activity of EPL-*g*-butyl@AgNPs. As shown in Figure 4, the inhibition zone diameters of EPL-*g*-butyl@AgNPs (16.74 mm for *S. aureus*, 16.6 mm for *P. aeruginosa*) were significantly larger than those of EPL-*g*-butyl (9.06 mm, 9.05 mm) and AgNPs (9.1 mm, 9.1 mm), indicating the synergistic antibacterial effect of EPL-*g*-butyl and AgNPs. The fractional inhibitory concentration index was calculated to be 0.1 for *P. aeruginosa* and 0.2 for *S. aureus*, which were both less than 0.5, demonstrating the synergistic antibacterial effects.

To confirm the antibacterial effect of EPL-*g*-butyl@AgNPs, live/dead assay was implemented by staining *P. aeruginosa* and *S. aureus*. The live bacterial cells with intact membranes appeared as green under fluorescence microscope, whereas the

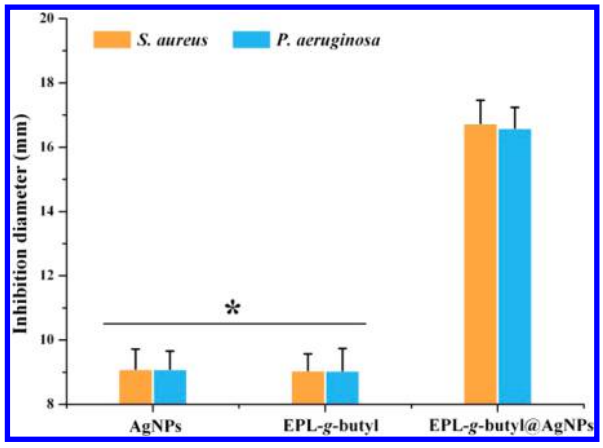

Figure 4. Inhibition zones of EPL-*g*-butyl@AgNPs, EPL-*g*-butyl, and AgNPs against *P. aeruginosa* and *S. aureus*.

dead cells with damaged membranes appeared to be red. In contrast to the green signals from live bacteria (Figures 5A and

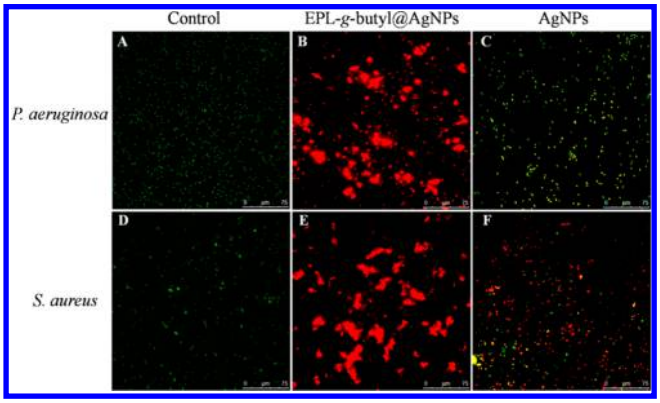

Figure 5. Fluorescence micrograph of bacteria after 1 h of treatment with antibacterial agents.

5D), cells were all dead and aggregated after treating with EPL-*g*-butyl@AgNPs for 1 h (Figures 5B and 5E). Figures 5C and 5F showed that a significant amount of bacterial cells were still alive without any aggregation after being treated with AgNPs for 1 h. Such a difference between ligand-modified and unmodified silver nanoparticles proved the superior role of the cationic polypeptide ligands—they actively bond to the bacterial surface and disrupted membrane structure. Taken together, EPL-*g*-butyl ligands exhibited direct multivalent interactions to bacteria, enabling the nanocomposites with superior antibacterial activity against both Gram-negative and Gram-positive bacteria.

Antibacterial Mechanism of EPL-*g*-Butyl@AgNPs. β-Galactosidase presented in *E. coli* was used as the study model to evaluate whether the nanocomposite can inhibit the activities of intracellular substances. β-Galactosidase catalyzes the enzymatic hydrolysis of ONPG to generate ONP. ONP can be recorded at 420 nm (OD_{420}) using UV−vis spectroscopy and used to monitor β-galactosidase activity. In the present work, cytoplasm solution was obtained from *E. coli* suspension by ultrasonication for 10 h at 0 °C following by filtration.[13] As shown in Figure 6, 34%, 57%, and 62% β-galactosidase activities were inhibited by different concentrations of EPL-*g*-butyl@AgNPs solution (0.9, 1.8, and 3.6 μg/mL), respectively, whereas 70% β-galactosidase activity was inhibited by 1.8 μg/

DOI: 10.1021/acsami.6b09267
ACS Appl. Mater. Interfaces 2016, 8, 25798−25807

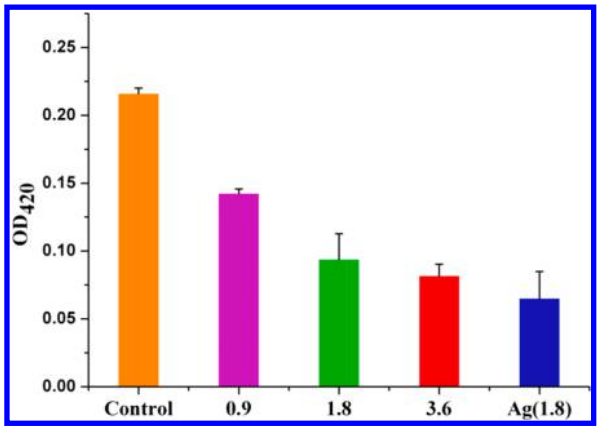

Figure 6. Absorptions of ONP at different concentrations.

mL AgNPs. It is speculated that AgNPs interacted effectively with the carboxyl and thiol groups of β-galactosidase, resulting in the denaturation of protein.[53,54] Although surface ligands reduced interactions between inner silver nanoparticles and proteins, the majority of β-galactosidase activity was still inhibited with increased concentrations. The inhibitory effect of silver nanoparticles on enzyme biological functions was also a major contribution to the superior antibacterial activities of the nanocomposites.

To further confirm membrane disruption mediated by the nanocomposites, morphological changes of Gram-negative (*P. aeruginosa*) and Gram-positive (*S. aureus*) bacteria isolates were observed by SEM after treated with EPL-*g*-butyl@AgNPs (28 μg/mL). The untreated bacteria with smooth and intact cell walls display rod- and round-shaped (Figures 7A and 7C). After 1 h EPL-*g*-butyl@AgNPs (Figures 7B and 7D) treatment, all cells exhibited partial or complete membrane lysis. The nanoparticles adsorbed to the negatively charged bacteria

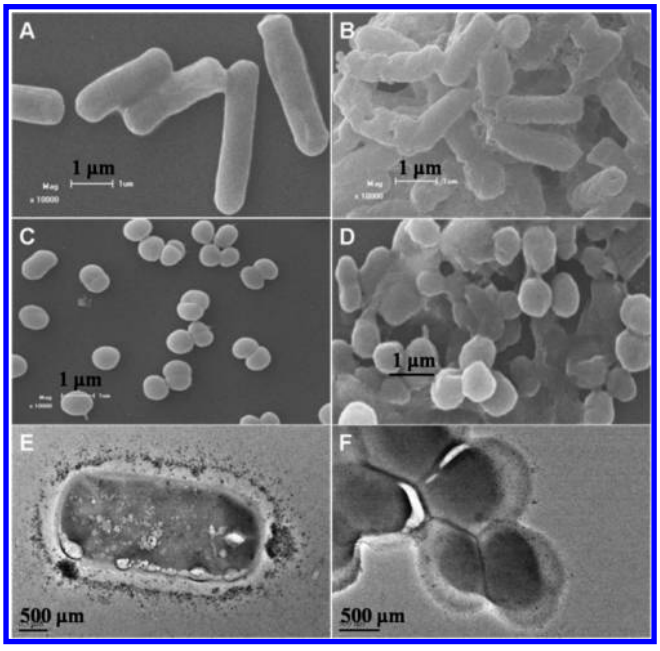

Figure 7. SEM images of *P. aeruginosa* and *S. aureus* before (A, C) and after (B, D) the treatment of EPL-*g*-butyl@AgNPs for 1 h. TEM images (E, F) of the EPL-*g*-butyl@AgNPs for *P. aeruginosa* and *S. aureus*, respectively.

surface through hydrophobic and electrostatic interactions, followed by interruption of cell walls and membranes, and finally led to cell death. Although the backbone of cell walls remained recognizable, large amounts of bacterial debris as well as bleb-like structures were observed, suggesting the cell wall destruction, similarly as previous reports.[55,56] TEM was also used to characterize the bacteria nanocomposite interactions. After being treated with EPL-*g*-butyl@AgNPs for 1 h, the nanocomposites were apparently well anchored on the bacterial cell surface and the cell walls became wrinkled with fold and breakage (Figures 7E and 7F). In summary, all these results revealed that the antibacterial activity of EPL-*g*-butyl@AgNPs was achieved by anchoring on the bacterial cell surface, damaging the cell walls as well as membranes, inhibiting intracellular biological functions, and finally leading to the cell death.

Bacterial Resistance of EPL-*g*-Butyl@AgNPs. The emergence of bacterial resistance to conventional antibiotics presents a major problem in clinical settings. It is vital to investigate whether EPL-*g*-butyl@AgNPs have any tendency to trigger bacterial resistance. To explore the potential of the nanocomposites as long-lasting antibacterial agents, the nanocomposites and levofloxacin were introduced in culture of Gram-negative (*P. aeruginosa*) and Gram-postive (*S. aureus*) bacteria, respectively. After 30 passages, EPL-*g*-butyl@AgNPs remained the same MIC value as beginning, whereas the MIC value of levofloxacin increased from 0.64 to 78 μg/mL against *S. aureus* and from 3.2 to 156 μg/mL against *P. aeruginosa*. Compared with the antibiotic, no antimicrobial resistance was observed against EPL-*g*-butyl@AgNPs, which demonstrated a potential solution to control and prevent the drug resistance.

Cytotoxicity Assay. Since low cytotoxicity is a major criterion for successful medical materials and released silver ions are known to be cytotoxic to human cells,[57] it is essential to assess whether EPL-*g*-butyl@AgNPs are cytotoxic. As shown in Figure 8, NIH3T3 fibroblast cells maintained a viability of 80% after 2 days treatment with EPL-*g*-butyl@AgNPs at a concentration of 56 μg/mL, which exceeded 20-fold of the MIC levels against both *P. aeruginosa* and *S. aureus*. As a contrast, AgNPs showed obvious cytotoxicity to cells when the concentration was up to 56 μg/mL, indicating the positive role of surface ligands to improve silver nanoparticle biocompatibility. Similarly, Mei and coauthors found that bacitracin A and polymyxin E functionalized AgNPs displayed low toxicity against NIH3T3 cells but enhanced toxicity to bacteria cells.[13] This selective cytotoxicity may be explained by the fact that bacteria surfaces bare more negative charges than mammalian cells,[58] which possess stronger interactions with the polycationic ligands. In addition, cholesterol components in mammalian cell membranes help to stabilize the membrane structures, making them less sensitive to antimicrobial AgNPs.[59]

***In Vivo* Study.** To assess the antibacterial efficacy of EPL-*g*-butyl@AgNPs and AgNPs *in vivo*, we utilized diabetic rats with wounds on their back as model. Four wounds were made on each rat: the treatment group, the model group, the nanocomposites control group, and the blank control group. The concentrations of both EPL-*g*-butyl@AgNPs and AgNPs were kept the same at 28 μg/mL. We photographed the traumas on day 1, 5, 9, 13, and 18 and performed histological evaluations of the rat dermal wound tissues on the 9th and 18th day to examine the wound healing status and any potential side effects. As shown in Figure 9A–J, trauma sizes treated with

DOI: 10.1021/acsami.6b09267
ACS Appl. Mater. Interfaces 2016, 8, 25798–25807

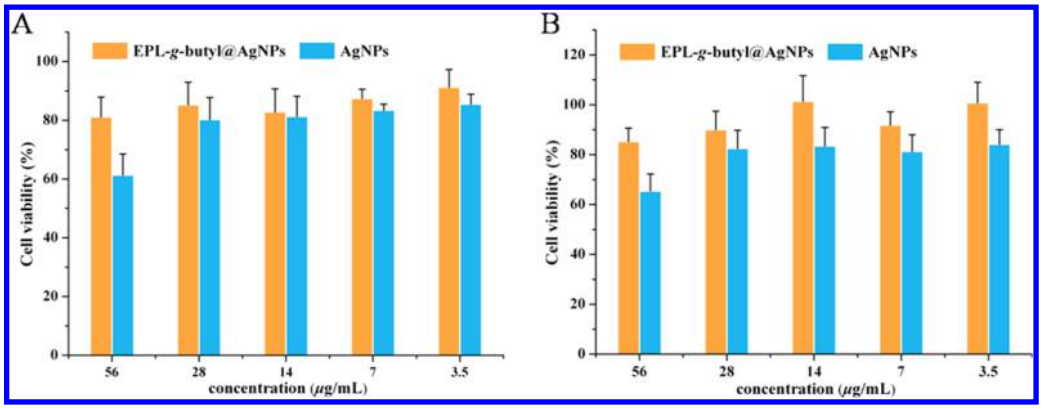

Figure 8. Cell viability of NIH 3T3 cells incubated with EPL-*g*-butyl@AgNPs and AgNPs for 1 (A) or 2 days (B).

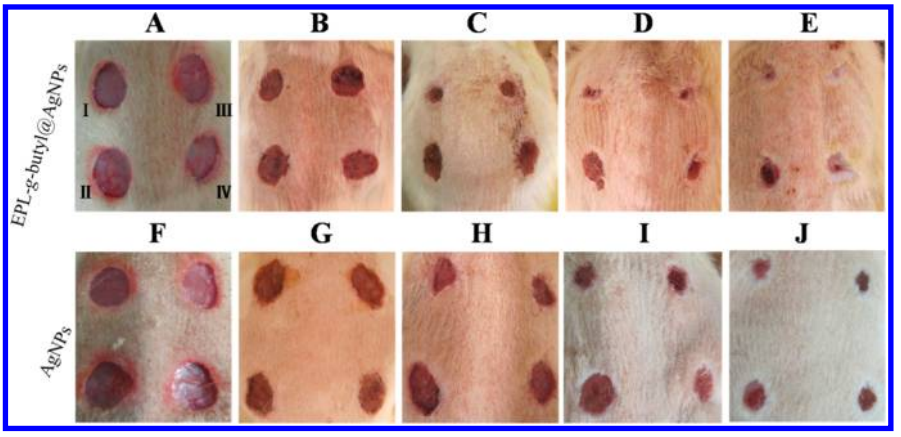

Figure 9. *In vivo* study on the effects of treatment of *P. aeruginosa* and *S. aureus*-induced wound infections for diabetic rats with EPL-*g*-butyl@AgNPs. Wound photographs of the rats taken at (A, F) day 1, (B, G) day 5, (C, H) day 9, (D, I) day 13, and (E, J) day 18.

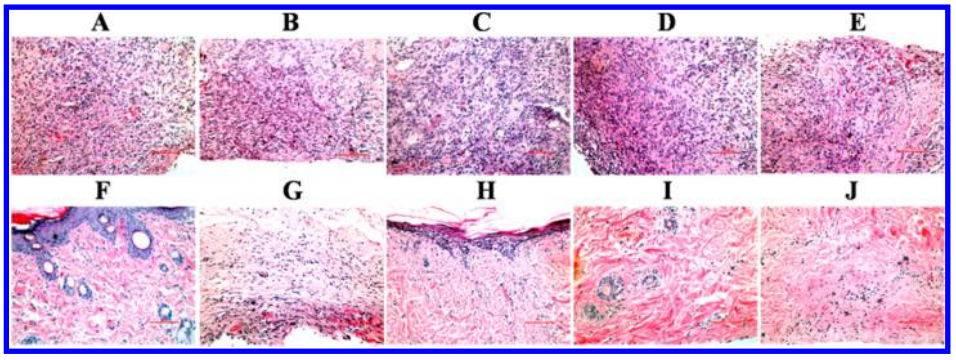

Figure 10. H&E staining of the rat dermal wound for EPL-*g*-butyl@AgNPs group (A, F), AgNPs group (B, G), model group (C, H), drug control group (D, I), and blank control group (E, J) after 9- and 18-day treatment, respectively.

both nanocomposites and AgNPs became smaller than those of model and blank control groups after 9-day treatment. After 18-day treatment, the wounds of the model group with the damaged immune systems were not healed well, whereas the wounds of all other groups healed significantly. Compared with AgNPs, the wounds treated with EPL-*g*-butyl@AgNPs healed faster (Figure 9).

To explore the host response against infection, wound tissues were harvested at the 9th and 18th day to perform hematoxylin and eosin-stained histological tests (Figure 10A–J).[13] After 9-day treatment, both the treatment and nanocomposite control groups had fewer inflammatory cells compared with model and blank control groups. After 18-day treatment, different signs of wound healing (epithelialization, granulation tissue formation, and contraction of wound) were observed for all groups except the model group (Figure 10F–J). The model group possessed mass inflammatory cells, suggesting that the wounds were still not recovered.

The damaged tissue may induce a cascade of events that promote wound repair, which includes formation of granulation tissues and re-epithelialization. This synergistic effort by the wounded cell layers is accompanied by a robust inflammatory response, in which inflammatory cells emigrate from systemic circulation and nearby tissues. The inflammation cells combat invading microbes and may also critically support the repair process by releasing a spectrum of cytokines and growth factors, which initiate the phase of tissue formation.[60,61] In the present work, we chose $CD68^+$ as the most reliable macrophage

DOI: 10.1021/acsami.6b09267
ACS Appl. Mater. Interfaces 2016, 8, 25798–25807

marker and $CD3^+$ T lymphocytes which play a significant role in a successful healing response.[62,63] $CD68^+$ macrophages and $CD3^+$ T cells were detected by immunohistochemical methods in wound tissues from all animal groups. As shown in Figure 11,

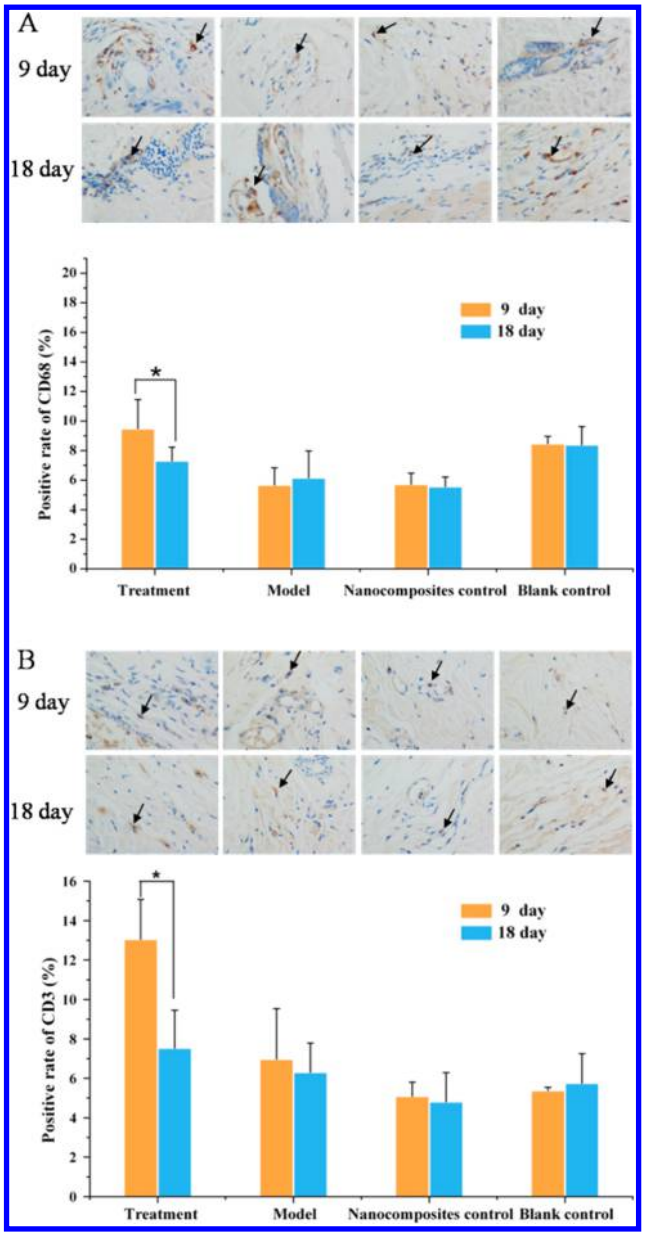

Figure 11. Photomicrographs of immune cell marker staining in the rat dermal wound: (A) positive rate of $CD68^+$; (B) positive rate of $CD3^+$ (400×).

the proportion of macrophages (9.5%) in the treatment group was significantly higher at the 9th day. Such high prevalence of macrophages promoted pro-inflammatory activities and helped to eradicate invading microorganisms. Similarly, the occurrence of $CD3^+$ T cells (13.1%) in the treatment group was significantly more frequent at the 9th day comparing with other groups. At the 18th day, the inflammatory cell proportions in treatment group significantly dropped compared with the 9th day values ($p < 0.05$), when the healing process was almost finished. Falanga reported an enhanced inflammation response in the wound healing process of diabetes mellitus therapy.[64] Jong and coauthors observed that administration of AgNPs in rats stimulated an increase in T cell populations.[65] In combination with the fact of rapid wound healing in the treatment group, our results suggested that the nanocomposites could modulate the relative density of specific immune cell subtypes. Taken together, the novel nanocomposites could trigger immune cells to congregate at wound site and thus fuel the immune response and promote wound healing.

CONCLUSIONS

In summary, we have successfully developed an effective antibacterial agent EPL-*g*-butyl@AgNPs by a one-pot synthesis strategy. Compared with AgNPs and EPL-*g*-butyl, the nanocomposites exerted polyvalent and synergistic antibacterial effects against both Gram-negative (*P. aeruginosa*) and Gram-positive (*S. aureus*) bacteria without emergence of bacterial resistance. The mechanism of antibacterial action of EPL-*g*-butyl@AgNPs was that the nanocomposites could bind to bacterial surface, followed by irreversibly disrupt cell wall as well as membrane structure, and subsequently penetrate cells and strongly inhibit enzyme activity, ultimately leading to bacteria apoptosis. Importantly, the nanocomposites showed good cytocompatibility toward NIH3T3 cells. *In vivo* tests using diabetic rat model proved that the nanocomposites could modulate inflammation cells thus promote wound healing without side effects on dermal tissues. This work improves our understanding of the antibacterial mechanism of AgNPs-based nanocomposites and offers an effective antibacterial agent for clinical applications.

ASSOCIATED CONTENT

Supporting Information

The Supporting Information is available free of charge on the ACS Publications website at DOI: 10.1021/acsami.6b09267.

Figure S1: ^{1}H NMR spectra of EPL and EPL-*g*-butyl in D_2O; Figure S2: FT-IR spectra of (a) EPL and (b) EPL-*g*-butyl; Figure S3: diameter distribution of EPL-*g*-butyl@AgNPs with different ratios of EPL-*g*-butyl to silver ion in aqueous solution: (A) 1:4, (B) 1:8, (C) 1:16, (D) 1:32, and (E) 1:64 (PDF)

AUTHOR INFORMATION

Corresponding Author

*Tel +86-22-23501645; Fax +86-22-23505598; e-mail zhangxinge@nankai.edu.cn (X.Z.).

Notes

The authors declare no competing financial interest.

ACKNOWLEDGMENTS

This publication is based on the work supported by the National Natural Science Foundation of China (Grants 21474055 and 51673102), Natural Science Foundation of Tianjin, China (Grant 14JYBJC29400), and the Specialized Research Fund for the Doctoral Program of Higher Education (Grant 20130031110014).

REFERENCES

(1) Kirby, T. Europe to Boost Development of New Antimicrobial Drugs. *Lancet* **2012**, *379*, 2229−2230.

(2) Lee, H.; Lee, Y.; Statz, A. R.; Rho, J.; Park, T. G.; Messersmith, P. B. Substrate-Independent Layer-by-Layer Assembly by Using Mussel-Adhesive-Inspired Polymers. *Adv. Mater.* **2008**, *20*, 1619−1623.

DOI: 10.1021/acsami.6b09267
ACS Appl. Mater. Interfaces 2016, 8, 25798−25807

(3) Li, P.; Zhou, C.; Rayatpisheh, S.; Ye, K.; Poon, Y. F.; Hammond, P. T.; Duan, H.; Chan-Park, M. B. Cationic Peptidopolysaccharides Show Excellent Broad-Spectrum Antimicrobial Activities and High Selectivity. *Adv. Mater.* **2012**, *24*, 4130−4137.
(4) Buffet-Bataillon, S.; Tattevin, P.; Bonnaure-Mallet, M.; Jolivet-Gougeon, A. Emergence of Resistance to Antibacterial Agents: The Role of Quaternary Ammonium Compounds−A Critical Review. *Int. J. Antimicrob. Agents* **2012**, *39*, 381−389.
(5) Some, S.; Ho, S. M.; Dua, P.; Hwang, E.; Shin, Y. H.; Yoo, H.; Kang, J. S.; Lee, D. K.; Lee, H. Dual Functions of Highly Potent Graphene Derivative-Poly-L-Lysine Composites to Inhibit Bacteria and Support Human Cells. *ACS Nano* **2012**, *6*, 7151−7161.
(6) Salick, D. A.; Pochan, D. J.; Schneider, J. P. Design of an Injectable Beta-Hairpin Peptide Hydrogel That Kills Methicillin-Resistant Staphylococcus Aureus. *Adv. Mater.* **2009**, *21*, 4120−4123.
(7) Li, Y.; Zhang, W.; Niu, J.; Chen, Y. Mechanism of Photogenerated Reactive Oxygen Species and Correlation with the Antibacterial Properties of Engineered Metal-Oxide Nanoparticles. *ACS Nano* **2012**, *6*, 5164−5173.
(8) Wu, M. C.; Deokar, A. R.; Liao, J. H.; Shih, P. Y.; Ling, Y. C. Graphene-Based Photothermal Agent for Rapid and Effective Killing of Bacteria. *ACS Nano* **2013**, *7*, 1281−1290.
(9) Zhao, Y.; Tian, Y.; Cui, Y.; Liu, W. W.; Ma, W. S.; Jiang, X. Small Molecule-Capped Gold Nanoparticles as Potent Antibacterial Agents That Target Gram-Negative Bacteria. *J. Am. Chem. Soc.* **2010**, *132*, 12349−12356.
(10) Qi, G.; Li, L.; Yu, F.; Wang, H. Vancomycin-Modified Mesoporous Silica Nanoparticles for Selective Recognition and Killing of Pathogenic Gram-Positive Bacteria over Macrophage-Like Cells. *ACS Appl. Mater. Interfaces* **2013**, *5*, 10874−10881.
(11) Ocsoy, I.; Paret, M. L.; Ocsoy, M. A.; Kunwar, S.; Chen, T.; You, M.; Tan, W. Nanotechnology in Plant Disease Management: DNA-Directed Silver Nanoparticles on Graphene Oxide as an Antibacterial against *Xanthomonas perforans*. *ACS Nano* **2013**, *7*, 8972−8980.
(12) Lu, Z. T.; Zhang, X. G.; Li, Z. Y.; Wu, Z. M.; Song, J.; Li, C. X. Composite Copolymer Hydrid Silver Nanoparticles: Preparation and Characterization of Antibacterial Activity and Cytotoxicity. *Polym. Chem.* **2015**, *6*, 772−779.
(13) Mei, L.; Lu, Z. T.; Zhang, X. G.; Li, C. X.; Jia, Y. X. Polymer-Ag Nanocomposites with Enhanced Antimicrobial Activity against Bacterial Infection. *ACS Appl. Mater. Interfaces* **2014**, *6*, 15813−15821.
(14) Regiel-Futyra, A.; Kus-Liśkiewicz, M.; Sebastian, V.; Irusta, S.; Arruebo, M.; Stochel, G.; Kyziol, A. Development of Noncytotoxic Chitosan-Gold Nanocomposites as Efficient Antibacterial Materials. *ACS Appl. Mater. Interfaces* **2015**, *7*, 1087−1099.
(15) Wang, H. Y.; Hua, X. W.; Wu, F. G.; Li, B.; Liu, P. D.; Gu, N.; Wang, Z. F.; Chen, Z. Synthesis of Ultrastable Copper Sulide Nanoclusters via Trapping the Reaction Intermediate: Potential Anticancer and Antibacterial Applications. *ACS Appl. Mater. Interfaces* **2015**, *7*, 7082−7092.
(16) Paladini, F.; Pollini, M.; Sannino, A.; Ambrosio, L. Metal-Based Antibacterial Substrates for Biomedical Applications. *Biomacromolecules* **2015**, *16*, 1873−1885.
(17) de Faria, A. F.; Perreault, F.; Shaulsky, E.; Chavez, L. H. A.; Elimelech, M. Antimicrobial Electrospun Biopolymer Nanofiber Mats Functionalized with Graphene Oxide-Silver Nanocomposites. *ACS Appl. Mater. Interfaces* **2015**, *7*, 12751−12759.
(18) Schiffman, J. D.; Wang, Y.; Giannelis, E. P.; Elimelech, M. Biocidal Activity of Plasma Modified Electrospun Polysulfone Mats Functionalized with Polyethyleneimine-Capped Silver Nanoparticles. *Langmuir* **2011**, *27*, 13159−13164.
(19) Feng, Q. L.; Wu, J.; Chen, G. Q.; Cui, F. Z.; Kim, T. N.; Kim, J. O. A Mechanistic Study of the Antibacterial Effect of Silver Ions on *Escherichia coli* and *Staphylococcus aureus*. *J. Biomed. Mater. Res.* **2000**, *52*, 662−668.
(20) Sambhy, V.; MacBride, M. M.; Peterson, B. R.; Sen, A. Silver Bromide Nanoparticle/Polymer Composites: Dual Action Tunable Antimicrobial Materials. *J. Am. Chem. Soc.* **2006**, *128*, 9798−9808.
(21) Liu, Z.; Yan, J.; Miao, Y.-E.; Huang, Y.; Liu, T. Catalytic and Antibacterial Activities of Green-Synthesized Silver Nanoparticles on Electrospun Polystyrene Nanofiber Membranes Using Tea Polyphenols. *Composites, Part B* **2015**, *79*, 217−223.
(22) Panáček, A.; Kvítek, L.; Prucek, R.; Kolář, M.; Večeřová, R.; Pizúrová, N.; Sharma, V. K.; Nevěčná, T.; Zbořil, R. Silver Colloid Nanoparticles: Synthesis, Charaterization, and Their Antibacterial Activity. *J. Phys. Chem. B* **2006**, *110*, 16248−16253.
(23) Deng, Z.; Zhu, H.; Peng, B.; Chen, H.; Sun, Y.; Gang, X.; Jin, P.; Wang, J. Synthesis of PS/Ag Nanocomposite Spheres with Catalytic and Antibacterial Activities. *ACS Appl. Mater. Interfaces* **2012**, *4*, 5625−5632.
(24) Popa, M.; Pradell, T.; Crespo, D.; Calderon-Moreno, J. M. Stable Silver Colloidal Dispersions Using Short Chain Polyethylene Glycol. *Colloids Surf., A* **2007**, *303*, 184−190.
(25) Chou, K. S.; Ren, C. Y. Synthesis of Nanosized Silver Particles by Chemical Reduction Method. *Mater. Chem. Phys.* **2000**, *64*, 241−246.
(26) Huang, H. H.; Ni, X. P.; Loy, G. L.; Chew, C. H.; Tan, K. L.; Loh, F. C.; Deng, J. F.; Xu, G. Q. Photochemical Formation of Silver Nanoparticles in Poly(N-vinylpyrrolidone). *Langmuir* **1996**, *12*, 909−912.
(27) Heckel, J. C.; Kisley, L. M.; Mannion, J. M.; Chumanov, G. Synthesis and Self-Assembly of Polymer and Polymer-Coated Ag Nanoparticles by the Reprecipitation of Binary Mixtures of Polymers. *Langmuir* **2009**, *25*, 9671−9676.
(28) Chen, M.; Wang, L. Y.; Han, J. T.; Zhang, J. Y.; Li, Z. Y.; Qian, D. J. Preparation and Study of Polyacryamide-Stabilized Silver Nanoparticles through a One-Pot Process. *J. Phys. Chem. B* **2006**, *110*, 11224−11231.
(29) Chen, M.; Zhao, Y.; Yang, W.; Yin, M. UV-Irradiation-Induced Templated/In-Situ Formation of Ultrafine Silver/Polymer Hybrid Nanoparticles as Antibacterial. *Langmuir* **2013**, *29*, 16018−16024.
(30) Chou, C. W.; Hsu, S.; Chang, H.; Tseng, S. M.; Lin, H. R. Enhanced Thermal and Mechanical Properties and Biostability of Polyurethane Containing Silver Nanoparticles. *Polym. Degrad. Stab.* **2006**, *91*, 1017−1024.
(31) Kong, H.; Jang, J. Antibacterial Properties of Novel Poly(methyl methacrylate) Nanofiber Containing Silver Nanoparticles. *Langmuir* **2008**, *24*, 2051−2056.
(32) Zhang, Q. M.; Serpe, M. J. Synthesis, Characterization, and Antibacterial Properties of a Hydroxyapatite Adhesive Block Copolymer. *Macromolecules* **2014**, *47*, 8018−8025.
(33) Fortunati, E.; Mattioli, S.; Visai, L.; Imbriani, M.; Fierro, J. L. G.; Kenny, J. M.; Armentano, I. Combined Effects of Ag Nanoparticles and Oxygen Plasma Treatment on PLGA Morphological, Chemical, and Antibacterial Properties. *Biomacromolecules* **2013**, *14*, 626−636.
(34) Kumar, P.; Ansari, K. B.; Koli, A. C.; Gaikar, V. G. Sorption Behavior of Thiourea-Grafted Polymeric Resin toward Silver Ion, Reduction to Silver Nanoparticles, and Their Antibacterial Properties. *Ind. Eng. Chem. Res.* **2013**, *52*, 6438−6445.
(35) Zimoch-Korzycka, A.; Jarmoluk, A. The Use of Chitosan, Lysozyme, and the Nano-Silver as Antimicrobial Ingredients of Edible Protective Hydrosols Applied into the Surface of Meat. *J. Food Sci. Technol.* **2015**, *52*, 5996−6002.
(36) Chang, Y. H.; Mclandsborough, L.; McClements, D. J. Interactions of a Cationic Antimicrobial (ε-Polylysine) with an Anionic Biopolymer (Pectin): An Isothermal Titration Calorimetry, Mocroelectrophoresis, and Turbidity Study. *J. Agric. Food Chem.* **2011**, *59*, 5579−5588.
(37) Timofeeva, L.; Kleshcheva, N. Antimicrobial Polymers: Mechanism of Action, Factors of Activity, and Applications. *Appl. Microbiol. Biotechnol.* **2011**, *89*, 475−492.
(38) Dai, X. M.; An, J. X.; Wang, Y. N.; Wu, Z. M.; Zhao, Y.; Guo, Q. Q.; Zhang, X. G.; Li, C. X. Antibacterial Amphiphiles Based on ε-Polylysine: Synthesis, Mechanism of Action, and Cytotoxicity. *RSC Adv.* **2015**, *5*, 69325−69333.
(39) Mei, L.; Lu, Z. T.; Zhang, W.; Wu, Z. M.; Zhang, X. G.; Wang, Y. N.; Luo, Y. T.; Li, C. X.; Jia, Y. X. Bioconjugated Nanoparticles for

DOI: 10.1021/acsami.6b09267
ACS Appl. Mater. Interfaces 2016, 8, 25798−25807

Attachment and Penetration into Pathogenic Bacteria. *Biomaterials* **2013**, *34*, 10328−10337.
(40) Kumar, S. N.; Siji, J. V.; Nambisan, B.; Mohandas, C. Activity and Synergistic Interactions of Stilbenes and Antibiotic Combinations against Bacteria *in Vitro*. *World J. Microbiol. Biotechnol.* **2012**, *28*, 3143−3150.
(41) Shome, A.; Dutta, S.; Maiti, S.; Das, P. K. In Situ Synthesized Ag Nanoparticle in Self-Assemblies of Amino Acid Based Amphiphilic Hydrogelators: Development of Antibacterial Soft Nanocomposites. *Soft Matter* **2011**, *7*, 3011−3022.
(42) Zhou, Z. X.; Wei, D. F.; Guan, Y.; Zheng, A. N.; Zhong, J. J. Damage of *Escherichia Coli* Membrane by Bactericidal Agent Polyhexamethylene Guanidine Hydrochloride: Micrographic Evidences. *J. Appl. Microbiol.* **2009**, *108*, 898−907.
(43) Tang, J.; Chen, Q.; Xu, L. G.; Zhang, S.; Feng, L. Z.; Cheng, L.; Xu, H.; Liu, Z.; Peng, R. Graphene Oxide-Silver Nanocomposite As a Highly Effective Antibacterial Agent with Species-Specific Mechanisms. *ACS Appl. Mater. Interfaces* **2013**, *5*, 3867−3874.
(44) Yang, J.; Balasundaram, G.; Lo, S.-L.; Guang, E. C. S.; Xue, J. M.; Song, J.; Wan, A. C. A.; Ying, J. Y.; Wang, S. Microfibers Fabricated by Non-Covalent Assembly of Peptide and DNA for Viral Vector Encapsulation and Cancer Therapy. *Adv. Mater.* **2012**, *24*, 3280−3284.
(45) Huang, W. J.; Niu, H. S.; Lin, M. H.; Cheng, J. T.; Hsu, F. L. Antihyperglycemic Effect of Catalpol in Streptozotocin-Induced Diabetic Rats. *J. Nat. Prod.* **2010**, *73*, 1170−1172.
(46) Ibrahim, A. A. E. Immunomodulatory Effects of Royal Jelly on Aorta CD3, CD68 and eNOS Expression in Hypercholesterolaemic Rats. *J. Basic. Appl. Zool.* **2014**, *67*, 140−148.
(47) Yang, T.; Yang, H.; Zhen, S. J.; Huang, C. Z. Hydrogen-Bond-Mediated in Situ Fabrication of AgNPs/Agar/PAN Electrospun Nanofibers as Reproducible SERS Substrates. *ACS Appl. Mater. Interfaces* **2015**, *7*, 1586−1594.
(48) Arvizo, R. R.; Saha, S.; Wang, E. F.; Robertson, J. D.; Bhattacharya, R.; Mukherjee, P. Inhibition of Tumor Growth and Metastasis by a Self-Therapeutic Nanoparticle. *Proc. Natl. Acad. Sci. U. S. A.* **2013**, *110*, 6700−6705.
(49) Zhao, Y. Y.; Tian, Y.; Cui, Y.; Liu, W. W.; Ma, W. S.; Jiang, X. Y. Small Molecule-Capped Gold Nanoparticles as Potent Antibacterial Agents That Target Gram-Negative Bacteria. *J. Am. Chem. Soc.* **2010**, *132*, 12349−12356.
(50) Huskens, J. Multivalent Interactions at Interfaces. *Curr. Opin. Chem. Biol.* **2006**, *10*, 537−543.
(51) Lin, C.-C.; Yeh, Y.-C.; Yang, C.-Y.; Chen, G.-F.; Chen, Y.-C.; Wu, Y.-C.; Chen, C.-C. Quantitative Analysis of Multivalent Interactions of Carbohydrate-Encapsulated Gold Nanoparticles with Concanavalin A. *Chem. Commun.* **2003**, 2920−2921.
(52) Pakulska, M. M.; Miersch, S.; Shoichet, M. S. Designer Protein Delivery: From Natural to Engineered Affinity-Controlled Release Systems. *Science* **2016**, *351*, 4750.
(53) Alt, V.; Bechert, T.; Steinrücke, P.; Wagener, M.; Seidel, P.; Dingeldein, E.; Domann, E.; Schnettler, R. An *in Vitro* Assessment of the Antibacterial Properties and Cytotoxicity of Nanoparticulate Silver Bone Cement. *Biomaterials* **2004**, *25*, 4383−4391.
(54) Huang, W.; Sher, Y. P.; Peck, K.; Fung, Y. C. Matching Gene Activity with Physiological Functions. *Proc. Natl. Acad. Sci. U. S. A.* **2002**, *99*, 2603−2608.
(55) Hao, Q. R.; Wang, H.; Wang, J.; Dou, J.; Zhang, M.; Zhou, W. D.; Zhou, C. L. Effective Antimicrobial Activity of Cbf-K_{16} and Cbf-A_7A_{13} against NDM-1-Carrying *Escherichia coli* by DNA Binding after Penetrating the Cytoplasmic Membrane *in Vitro*. *J. Pept. Sci.* **2013**, *19*, 173−180.
(56) Ma, L.; Wang, Y.; Wang, M.; Tian, Y.; Kang, W.; Liu, H.; Wang, H.; Dou, J.; Zhou, C. Effective Antimicrobial Activity of Cbf-14, Derived from a Cathelin-Like Domain, against Penicillin-Resistant Bacteria. *Biomaterials* **2016**, *87*, 32−45.
(57) Beer, C.; Foldbjerg, R.; Hayashi, Y.; Sutherland, D. S.; Autrup, H. Toxicity of Silver Nanoparticles-Nanoparticle or Silver Ion? *Toxicol. Lett.* **2012**, *208*, 286−292.
(58) Matsuzaki, K. Control of Cell Selectivity of Antimicrobial Peptides. *Biochim. Biophys. Acta, Biomembr.* **2009**, *1788*, 1687−1692.
(59) Matsuzaki, K.; Sugishita, K.; Fujii, N.; Miyajima, K. Molecular-Basis for Membrane Selectivity of an Antimicrobial Peptide, Magainin-2. *Biochemistry* **1995**, *34*, 3423−3429.
(60) Martin, P.; Leibovich, S. J. Inflammatory Cells During Wound Repair: the Good, the Bad and the Ugly. *Trends Cell Biol.* **2005**, *15*, 599−607.
(61) Eming, S. A.; Hammerschmidt, M.; Krieg, T.; Roers, A. Interrelation of Immunity and Tissue Repair or Regeneration. *Semin. Cell Dev. Biol.* **2009**, *20*, 517−527.
(62) Wamala, I.; Matar, A. J.; Farkash, E.; Wang, Z.; Huang, C. A.; Sachs, D. H. Recombinant Anti-Monkey CD3 Immunotoxin Depletes Peripheral Lymph Node T Lymphocytes More Effectively than Rabbit Anti-Thymocyte Globulin in Naïve Baboons. *Transplant Immunol.* **2013**, *29*, 60−63.
(63) Sjödahl, G.; Lövgren, K.; Lauss, M.; Chebil, G.; Patschan, O.; Gudjonsson, S.; Månsson, W.; Fernö, M.; Leandersson, K.; Lindgren, D.; Liedberg, F.; Höglund, M. Infiltration of $CD3^+$ and $CD68^+$ Cells in Bladder Cancer is Subtype Specific and Affects the Outcome of Patients with Muscle-Invasive Tumors. *Eur. Urol. Suppl.* **2014**, *32*, 791−797.
(64) Falanga, V. Wound Healing and Its Impairment in the Diabetic Foot. *Lancet* **2005**, *366*, 1736−1722.
(65) De Jong, W. H.; Van Der Ven, L. T. M.; Sleijffers, A.; Park, M. V. D. Z.; Jansen, E. H. J. M.; Van Loveren, H.; Vandebriel, R. J. Systemic and Immunotoxicity of Silver Nanoparticles in An Intravenous 28 Days Repeated Dose Toxicity Study in Rats. *Biomaterials* **2013**, *34*, 8333−8343.

DOI: 10.1021/acsami.6b09267
ACS Appl. Mater. Interfaces 2016, 8, 25798−25807